Sensors and Actuators B 243 (2017) 1083–1091

Contents lists available at ScienceDirect

Sensors and Actuators B: Chemical

journal homepage: www.elsevier.com/locate/snb

Fabrication of well-ordered porous array mounted with gold nanoparticles and enhanced sensing properties for mixed potential-type zirconia-based NH_3 sensor

Bin Wang[b], Shiting Yao[b], Fangmeng Liu[b], Yehui Guan[b], Xidong Hao[b], Xishuang Liang[a,b,*], Fengmin Liu[b], Peng Sun[b], Yue Wang[c], Hongwei Song[b], Geyu Lu[a,b,*]

[a] State Key Laboratory of Automotive Simulation and Control, Jilin University, 5988 Renmin Avenue, Changchun 130012, China
[b] State Key Laboratory on Integrated Optoelectronics, College of Electronic Science and Engineering, Jilin University, 2699 Qianjin Street, Changchun 130012, China
[c] State Key Laboratory of Supramolecular Structure and Materials, Jilin University, 2699 Qianjin Street, Changchun 130012, China

ARTICLE INFO

Article history:
Received 25 July 2016
Received in revised form 3 December 2016
Accepted 18 December 2016
Available online 20 December 2016

Keywords:
YSZ
NH_3 sensor
Three-phase boundary
Gold nanoparticle
PS sphere
SnO_2

ABSTRACT

The nano-bowl shaped structure and gold nanoparticle array were successfully fabricated on the YSZ substrate and examined to improve the sensitivity of mixed potential type NH_3 gas sensor. The nano-bowl shaped structure was constructed by solution-dipping template (polystyrene spheres) strategy and gold nanoparticle inlaid in the nanostructure was fabricated by vacuum evaporation plating technology. The present study mainly explored the influence of gold layer's thickness on the nanostructure. The perfect ordered gold nanoparticle array inlaid in nano-bowl shaped structure was obtained when the evaporated gold film thickness was about 50 nm. The mixed potential type gas sensor which based on processed YSZ substrate displayed the improved sensitivity and selectivity to NH_3 at elevated temperature. All the enhanced sensing properties might due to the enlarged three phase boundary (TPB) and inlaid gold nanoparticle array.

1. Introduction

Selective catalyst reduction (SCR) systems have been widely used in diesel cars to eliminate the NO_x emissions. In this system, the NO_x is removed by a chemical reaction with NH_3: $2NO + 4NH_3 + 2O_2 = 3N_2 + 6H_2O$ [1–3]. However, the emission of NH_3 to environment is also harmful. Thus, developing a NH_3 gas sensor to prevent the release of unreacted NH_3 in SCR is becoming more important.

Yttria-stabilized zirconia (YSZ)-based gas sensor, famous for its chemical and mechanical stability [4–7], has been widely used in monitoring vehicle emission. The sensitivities of this type gas sensor were mainly affected by the sensing electrode material and the structure of the three-phase boundary (TPB). Various materials such as single and mixed oxides were used as sensing material and presented good sensitivities. Liu et al. used In_2O_3 as sensing material fabricated the sensor and showed a good sensitivity to NO_2 at 700 °C [8]. Au doped metal oxides were also extensively studied as sensing electrode material. Elumalai et al. fabricated the YSZ-based sensor utilizing Au/NiO composite sensing-electrode and gave selective and sensitive response to C_3H_6 [9]. Wu et al. developed CO gas sensor based on YSZ and Au-doped Ga_2O_3 sensing electrode at high temperature [10]. On the other hand, TPB also played an important role on the sensitivities of the sensor. High performance TPB means a larger contact area between sensing electrode material, YSZ substrate and the sample gas, which could provide more electrochemical reaction active sites for the electrochemical reaction. A series of methods such as sand blasting technology [11], hydrofluoric acid corrosion [12] and femtosecond laser direct writing technology [13] were used to construct an efficient TPB. In our previous work, by using PS spheres (PSs) as a template combined with solution-dipping method [14–18], nano-bowl shaped structure was successfully fabricated on the YSZ substrate. The sensing properties of the sensor which using processed YSZ substrate as electrolyte showed a significant enhancement to NO_2 [19]. Up to now, there are a few related reports about constructing gold nanoparticle inlaid in nano-bowl shaped structure on the YSZ substrate. The design of such nanostructure array not only enlarged the TPB but also introduced the gold nanoparticles into sensing

* Corresponding authors at: State Key Laboratory of Automotive Simulation and Control, Jilin University, 5988 Renmin Avenue, Changchun 130012, China.
E-mail addresses: liangxs@jlu.edu.cn (X. Liang), lugy@jlu.edu.cn (G. Lu).

http://dx.doi.org/10.1016/j.snb.2016.12.094
0925-4005/

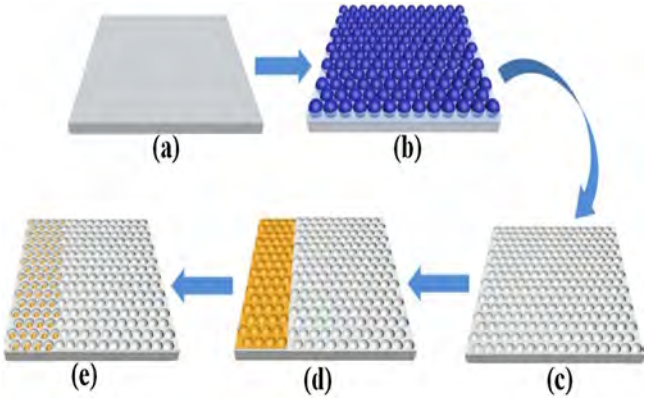

Fig. 1. Schematic illustration of the fabrication strategy for well-ordered porous array mounted with gold nanoparticles.

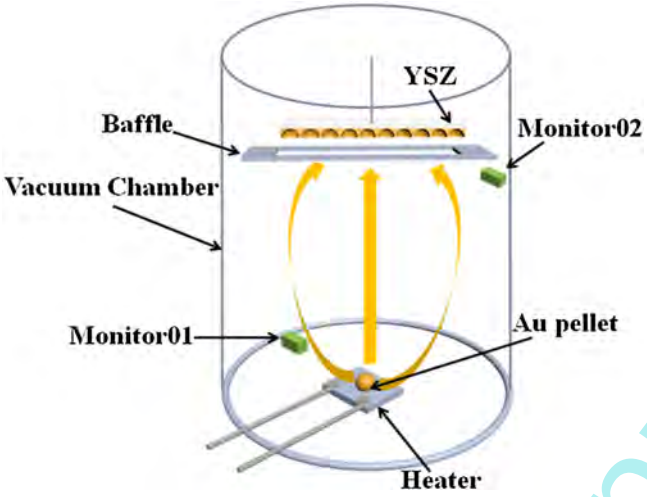

Fig. 2. Diagram of vacuum evaporator.

electrode, which could significantly enhance the sensitivities of sensor.

In this paper, the well-ordered nano-bowl shaped structure and gold nanoparticle array was fabricated on the YSZ substrate by solution dipping method and vacuum evaporation plating technology, respectively. The high performance mixed-potential type NH_3 sensor utilizing the processed YSZ substrate as electrolyte and SnO_2 as sensing electrode material was fabricated and tested.

2. Experimental

2.1. Fabrication of well-ordered porous array mounted with gold nanoparticles

The process of fabricating gold nanoparticles on the YSZ substrate was shown in Fig. 1. As we reported before, the nano-bowl shaped structure was fabricated on the YSZ substrate successfully by the solution dipping PSs template strategy. After solution dipping, the PSs template was picked up by YSZ substrate. Then the substrate was annealing at 1300 °C for 3 h to remove PSs template. The processed YSZ substrate was introduced into the vacuum chamber (Organic metal vapor deposition system, LN-1046SC) and was fixed between two independent evaporation rate monitors, as shown in Fig. 2. Monitor01 was put close to the gold pellet (purity is 99.99%) to monitor the evaporation rate of gold. Monitor02 was used to show the deposition rate of gold. These two monitors allow us to estimate the final thickness of the gold film by controlling the

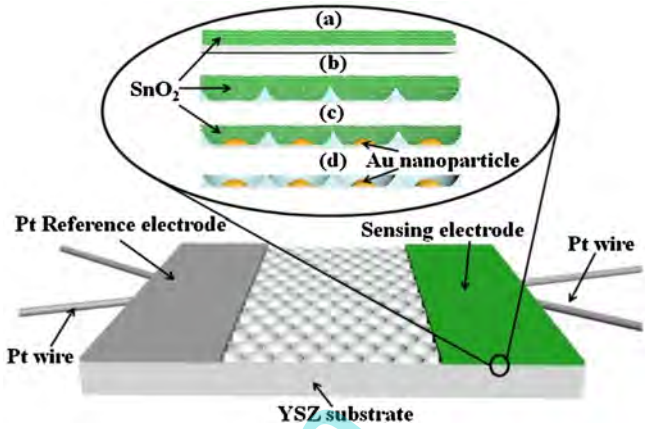

Fig. 3. Schematic diagram of the YSZ-based NH_3 sensors.

evaporation time. When the evaporation rate monitored by monitor01 was maintained, the baffle was removed and gold started evaporated onto the YSZ substrate at the rate of 0.5 Å/s as shown in monitor02 [20,21]. By controlling evaporation time (200 s 400 s 1000 s 2000s), four different thickness gold films (10 nm, 20 nm, 50 nm, 100 nm) were prepared on the processed YSZ substrate. Then, the processed YSZ substrates covered with different thickness gold film were sintered at 1100 °C for 3 h, and the gold nanoparticle was successfully inlayed into the nano-bowl shaped structure.

2.2. Fabrication and measurement of the sensor

To further explore the influence of TPB and gold nanoparticle on the sensitivities of the sensor, four different YSZ-based NH_3 sensors were fabricated. The sensors using YSZ substrate with or without nanostructure porous nanostructure array film were labeled as S1 and S0 as illustrated in Fig. 3(a) and (b). The sensors based on the YSZ substrate which coated with gold nanostructure array covered or not covered SnO_2 sensing electrode material were labeled as S2 and S3 as shown in Fig. 3(c) and (d). SnO_2 sensing electrode material was prepared by sintering $SnCl_4$ at 800 °C for 3 h. The stripe-shaped Pt (0.5 mm × 2 mm) acted as the reference electrode (RE), the sensing electrode (SE) was fabricated through the point-shaped Pt (0.8 mm × 2 mm) covered by the SnO_2 layer. Then the devices were sintered at 800 °C for 3 h. Finally, the Pt heater was affixed on the back of YSZ substrate to offer the working temperature of the sensor.

For the mixed-potential type gas sensor, the response signal (ΔV) was the potential difference between sensing electrode and Pt reference electrode. When the sensor was exposed to sample gas, the potential change on sensing electrode is much larger than Pt reference electrode. The sensing properties of the sensor were measured by conventional static mounting static mounting method. The specific process as follows: The sample gas containing different NH_3 concentration were obtained by diluting 1% NH_3 with base gas (21 vol.% O_2 and 79% vol.% N_2). When the sensor exposed to sample gas or air, the sensing signal (ΔV) was measured by a digital electrometer (Digital Multimeter; Rigol Technologies, Inc., DM 3054, China), and the results were recorded into the computer which connected with the electrometer.

X-ray diffraction (XRD) was used to show the phase structure of sensing electrode material (SnO_2) (wavelength = 0.1541 nm). The morphology of the YSZ substrate and sensing electrode material were shown by Field emission scanning electron microcopy (SEM) using a JEOL JSM-7500F microscope with an accelerating voltage of 15 kV and atomic force microscope(AFM; Being Nano-Instrument, Ltd., CSPM5500, China). And the polarization curves were obtained

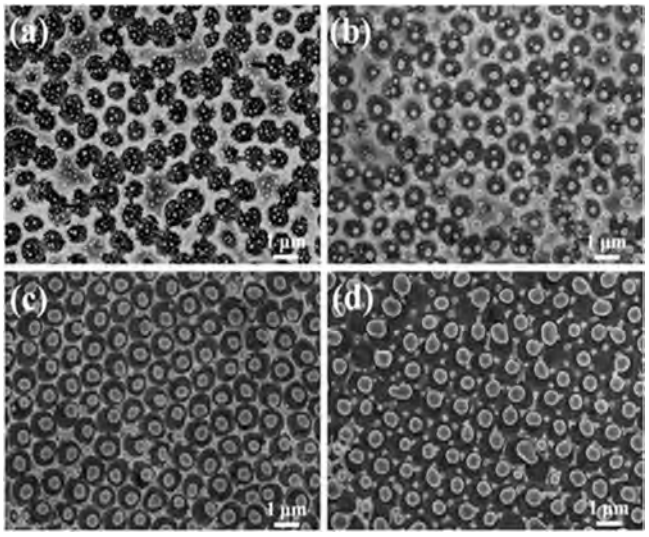

Fig. 4. SEM images of morphology of YSZ substrate coated with different thickness gold film (a) 10 nm (b) 20 nm (c) 50 nm (d) 100 nm after annealing at 1100 °C for 3 h.

by using electrochemical work station (CHI600C, Instrument Corporation of Shanghai, China).

3. Results and discussion

The thickness of 10 nm, 20 nm, 50 nm, 100 nm gold films were coated on the processed YSZ substrate by controlling the evaporating time, respectively. Fig. 4 showed SEM images of processed YSZ substrate coated with different thickness of gold film after annealing at 1100 °C for 3 h. Due to the surface tension and the uneven surface of YSZ substrate, the gold film would shear off during annealing process when the thickness of gold layer was relatively thin (10 nm or 20 nm). As a result, the number of gold nanoparticle in the nano-bowl shaped structure was uncertain and the distribution of gold nanoparticle is irregular as shown in Fig. 4(a) and (b). When the evaporated thickness of gold was about 50 nm, gold nanoparticle was successfully inlaid in the nano-bowl shaped structure on the YSZ substrate after annealing, and almost every gold nanoparticle take up a nano-bowl shaped structure (Fig. 4(c)). The specific geometry size of the gold nanoparticle could be obtained from AFM image as indicated in Fig. 5(a) and (b), the diameter of the nanoparticle is about 600 nm and the height of gold nanoparticle is approximately 160 nm. Furthermore, the nano-bowl shaped structure was badly destroyed and the shape of gold nanoparticle became irregular when the gold layer thickness increased to 100 nm, as illustrated in Fig. 4(d).

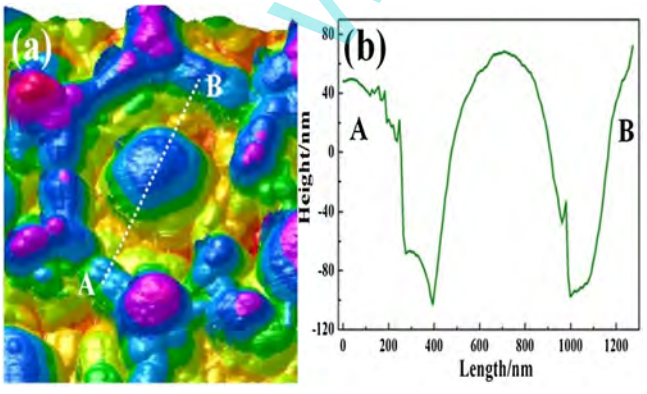

Fig. 5. (a) AFM image of nano-bowl shaped structure mounted gold nanoparticle; (b) the height variation curves of the cross-section.

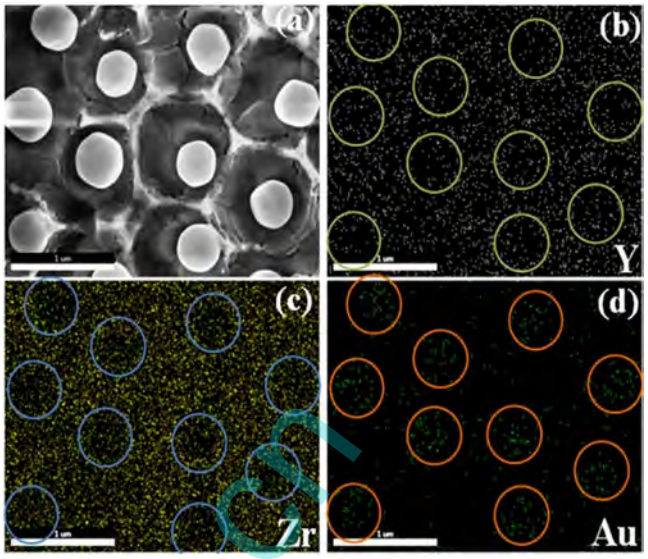

Fig. 6. (a) SEM images of the surface of YSZ substrate ordered porous array mounted with gold nanoparticles; EDS observation for the element of (b) Y (c) Zr (d) Au.

The EDS mapping images of the processed YSZ substrate were also measured to further illustrate distribution of Au element as shown in Fig. 6. EDS analysis indicated coexists of Y, Zr, and Au contents. After detail analysis, the places circled out in Fig. 6(b and c) were identified as gold nanoparticles because the signals of Y and Zr in the corresponding locations were pretty weak. Meanwhile, the signal of Au was regularly dispersed and concentrated in the places circled out in Fig. 6(d), which demonstrated that the gold had been perfectly filled in the nano-bowl shaped structure [22].

XRD measurement was carried out to confirm the composition and crystalline phase of SnO_2 sensing electrode material. Fig. 7(a) reveals the XRD pattern of SnO_2. All the diffraction peaks of SnO_2 were accorded well with the signal phase SnO_2 with tetragonal structure (JCPDS No. 88-287). No impurity phases were observed from the pattern, which suggests the high purity of material. The diameter of SnO_2 nanoparticle was about 24.2 nm according to Debye-Scherer formula. Fig. 7(b) shows the SEM image of nano-bowl shaped structure filled with SnO_2 nanoparticles. It could be seen that SnO_2 nanoparticles were successfully filled into the nano-bowl shaped structure and formed an efficient TPB.

The response and recovery properties of sensor S2 at different operating temperatures were exhibited in Fig. 8. The absolute value tended to increase with the initial increase in the temperature and the maximum response to 100 ppm NH_3 was obtained at 650 °C. At a higher temperature, the absolute value tended to decrease. Consequently, 650 °C was considered as the best operating temperature and was used in the subsequent sensitivity property tests.

The response transient curves of sensor S0, S1, S2, and S3 to 10–400 ppm NH_3 were showed in Fig. 9(a). Obviously, S2 generated the highest response to NH_3 at every concentration conditions. And S3 had the lowest response to NH_3 in the range of 10–400 ppm. For sensor S3, the gold nanoparticle array which fabricated on the YSZ substrate was considered had excellent catalyst to target gases. As a result, the response of sensor S3 to different concentrations of NH_3 changed little and generated sensitivity as −9.2 mV/decade as illustrated in Fig. 9(a) and (b). When SnO_2 sensing electrode material was prepared on the smooth surface YSZ substrate and fabricated the sensor (S0), the response of S0 to 100 ppm NH_3 was about −21.6 mV, which showed that SnO_2 had a certain catalytic activity to NH_3. When SnO_2 was covered on the processed YSZ sub-

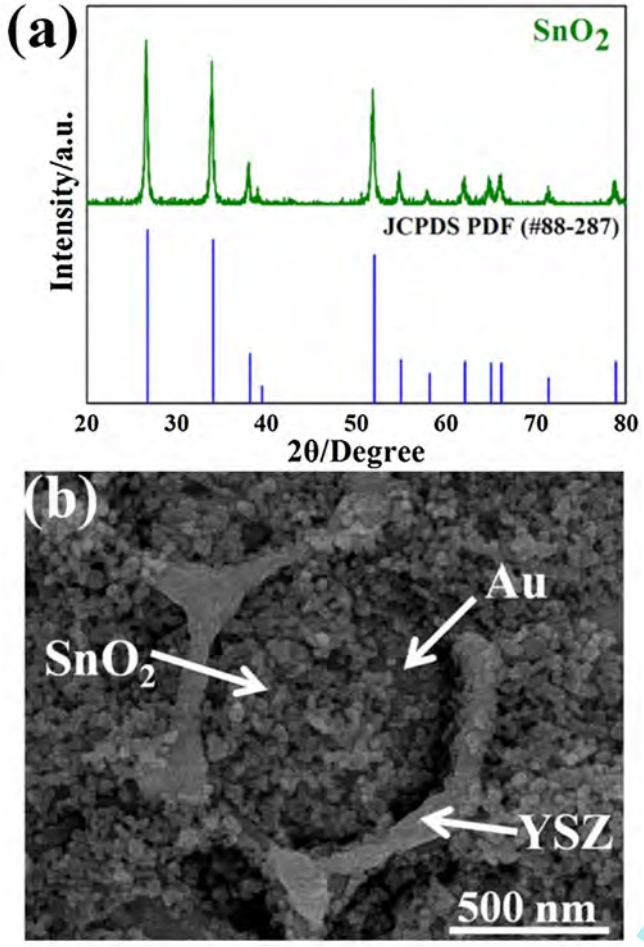

Fig. 7. (a) XRD pattern of SnO_2 sensing electrode material; (b) SEM image of YSZ substrate ordered porous array mounted with gold nanoparticles filled with SnO_2 sensing electrode material.

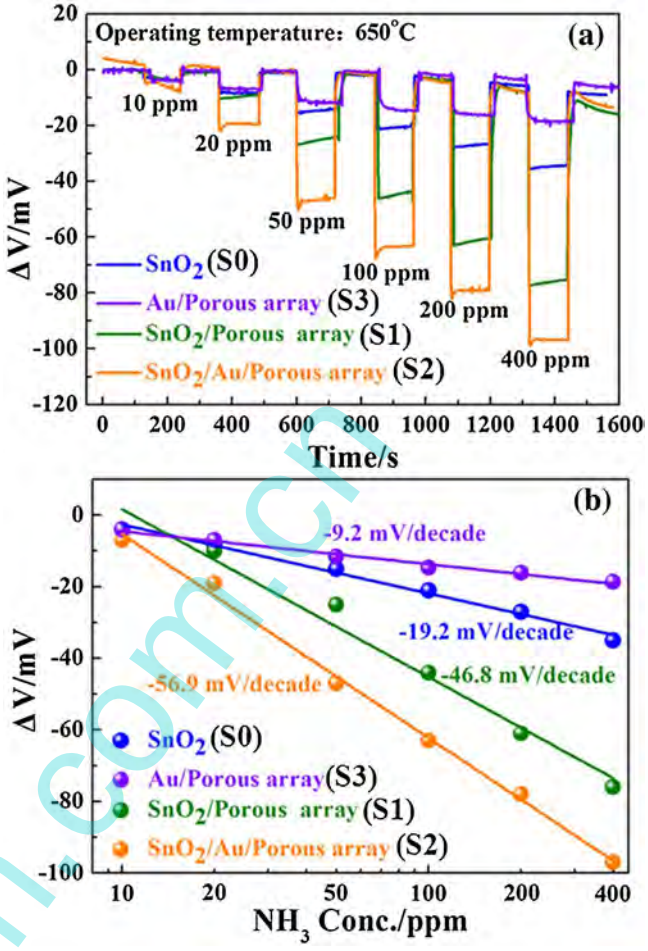

Fig. 9. (a) Response transient curves for the sensor S0, S1, S2, S3 to 10–400 ppm NH_3 at 650 °C; (b) dependence of ΔV on the logarithm of NH_3 concentrations for the sensors S0, S1, S2, S3 at 650 °C.

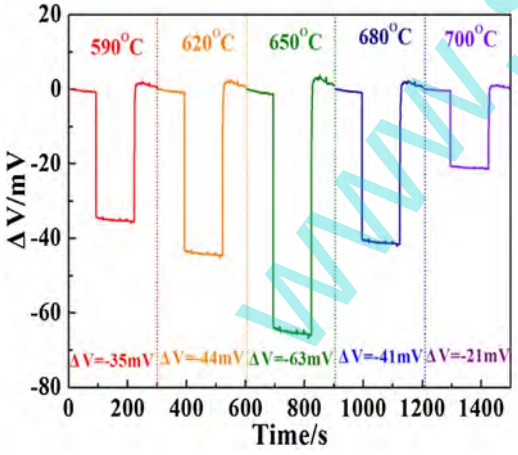

Fig. 8. The response of sensor S3 to 100 ppm NH_3 at different temperatures.

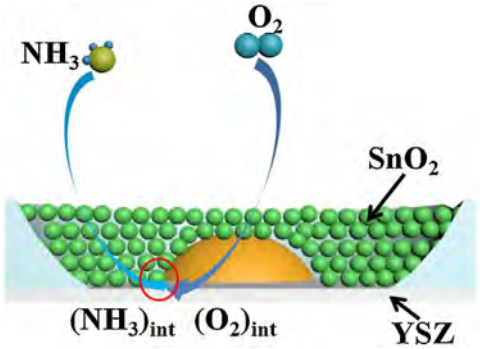

Fig. 10. Schematic representation of NH_3 sensing mechanism for the sensor S2.

strate and fabricated the sensor (S2), the sensitivity of S2 is highly enhanced as illustrated in Fig. 9(a). The reason for the enhanced sensitivity could be explained by the enlarged efficient TPB and the construction of gold nanoparticle array. TPB is a reaction region for the cathodic reaction: $1/2O_2 + 2e^- \rightarrow O^{2-}$ (1) and anodic reaction: $2/3NH_3 + O^{2-} \rightarrow 1/3N_2 + H_2O + 2e^-$ (2). The nano-bowl shaped structure fabricated on the YSZ substrate could provide a larger TPB, which makes the response of S2 to NH_3 highly enhanced compared with S0. The improved sensitivity of sensor S1 compared with S0 could also be explained by the enlarged TPB. The effect of gold nanoparticle array could be explained by the physico-chemical model [23]. The adsorption of oxygen could be expressed by the following equilibrium reactions (Fig. 10).

According to the equilibrium between oxygen vacancies and oxygen gas, the mechanism of electrical conduction in tin oxide could be written as follow:

$$O_2 + 2S_{ox} \rightarrow 2O\text{-}s_{ox}$$

$$O\text{-}s_{ox} + V_{\ddot{O}} + 2e_{ox} \rightarrow Oo^*$$

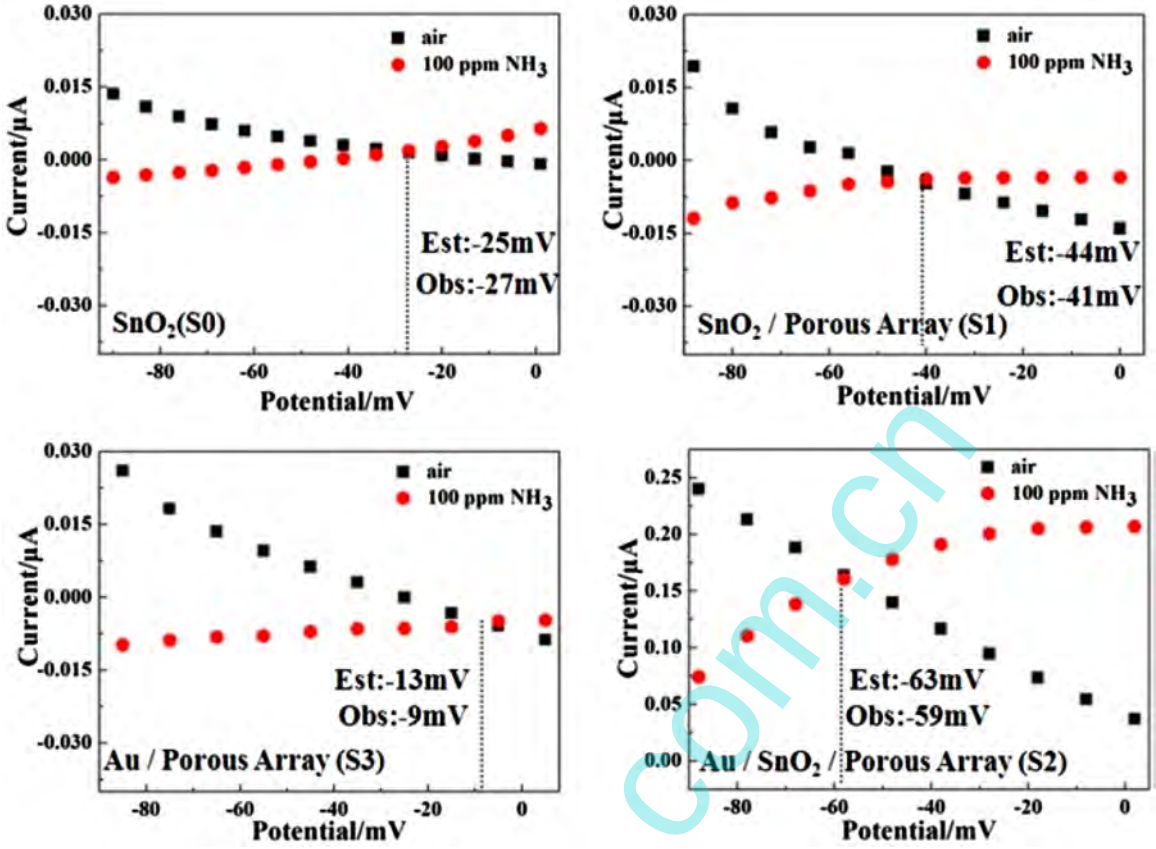

Fig. 11. Modified polarization curve in 100 ppm NH_3 and in air for the sensor S0, S1, S2, S3 operated at 650 °C.

$$O_2 + 2V_{\ddot{O}} + 4e_{ox} \rightarrow 2Oo^*$$

Where $V_{\ddot{O}}$ is oxygen vacancy, e_{ox} is the electron of tin oxide and Oo^* represent the lattice oxygen.

When the gold nanoparticle contact with tin oxide, the spillover effect and electron change between gold and tin oxide are two main factors affect the catalytic activation of oxygen dissociation [24–26]. The spillover effect could consist in catalytic activation of oxygen dissociation on SnO_2 according to the following equations:

$$O_2 + 2S_M \rightarrow 2O\text{-}s_M$$

$$O\text{-}s_M + e_{ox} + S_{ox} \rightarrow O^-\text{-}s_{ox} + S_M$$

Where S_M is an adsorption site on the metal, S_{ox} is an adsorption site on SnO_2. The second possible action of the gold in an electronic effect [27,28] consisting in electron change between metal and SnO_2 by following equations:

$$O_2 + 2e_M + 2S_M \rightarrow O^-\text{-}s_M$$

$$e_{ox} \rightarrow e_M$$

On the TPB, the oxygen transmission could be expressed by following equations:

$$O\text{-}s_{ox} + S_T \rightarrow O\text{-}s_T + S_{ox}$$

$$O\text{-}s_M + S_T \rightarrow O\text{-}s_T + S_M$$

Where S_T is the adsorption site on the TPB, $O\text{-}s_T$ is the adsorbed species on the TPB. With the construction of gold nanoparticle array, more oxygen would be adsorbed on TPB and accelerated electrochemical reaction [29,30]. Lu et al. reported that the particle size of Au nanoparticle would highly influence catalyst activity of CO oxidation reaction [31]. However, the influence of strain effect, length among gold-YSZ-SnO_2 on the sensing properties would be explored in the following experiment.

On the other hand, due to the strong acid-base interaction, NH_3 molecules could be absorbed on SnO_2 nanoparticle completely and then spillover to TPB. As a result, both cathodic and anodic reactions are accelerated at TPB and a larger response is generated [32]. To verify the sensing mechanism further, the polarization curves for sensor S0, S1, S2, S3 were measured (Fig. 11). The modified anodic polarization curves were obtained by subtracting current in air from in sample gas. The different variation range of polarization curves may be caused by different electrochemical reaction activity at TPB. The slope of anodic polarization curve for sensor S2 is much larger than other sensors, which represent a higher electrochemical reaction activity to NH_3. Besides, mixed-potential could also be estimated from the intersection point of anodic and cathodic polarization curves [33]. The mixed-potential mechanism could be verified by comparing mixed potential estimated values and observed values of experiment. The estimated values are essentially in agreement with the observed values to 100 ppm NH_3. These results show clearly that the sensors agree with the mixed-potential mechanism [34,35]. Fig. 9(b) shows the dependence of ΔV on the logarithm of NH_3 concentrations for the sensor S0, S1, S2, S3 at 650 °C. The ΔV for every sensor is almost linearly with logarithm of NH_3 concentration in the range of 10–400 ppm which is accordance with the mixed-potential mechanism. The slope of S2 was about −56.9 mV/decade, and other sensors S0, S1, S3 were approximately −19.2 mV/decade, −46.8 mV/decade, −9.2 mV/decade. Obviously, gold nanoparticle array and high-performance TPB played important roles in the enhancement of

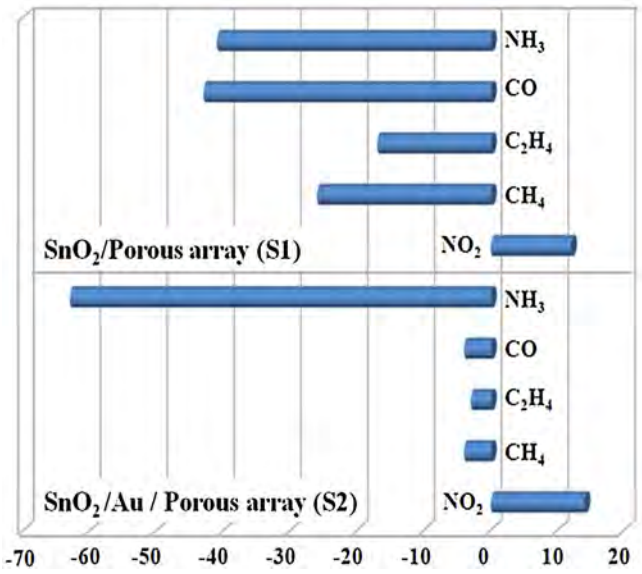

Fig. 12. Sensitivities of sensor S1 and S2 to 100 ppm various gases at 650 °C.

the sensitivity. Meanwhile, t_{res} and t_{rec} of S2 were about 1s, which showed excellent response and recovery performance.

The selectivities of S1 and S2 to various gases at 650 °C were illustrated in Fig. 12. It can be observed that the sensor S1 generated almost the same response to 100 ppm NH_3 and CO at 650 °C. Additionally, other gases such as C_2H_4 and CH_4 also had great impact on the detection of NH_3. However, the response of S2 to 100 ppm NH_3 was significantly increased and other examined gases decreased largely at 650 °C, which showed S2 displayed the enhanced selectivity to NH_3. In order to explain the effect of gold nanoparticle on the selectivity of the sensor, the polarization curves for S1 and S2 in sample gas (100 ppm NH_3 and 100 ppm CO) and in base gas (in air) at 650 °C were measured, respectively. The cathodic polarization curve of O_2 for the sensor S2 was largely increased with the presence of gold nanoparticle. The slope of polarization curve for NH_3 was much larger than CO as shown in Fig. 13, which demonstrated a higher electrochemical reaction activity of NH_3 at TPB [36]. These resulted in the increase in the response to NH_3 and decrease in the response to CO. Based on above reasons, the selectivity of the sensor S2 was largely improved with the presence of gold nanoparticle [37].

According to mixed-potential theory, the electrochemical reaction (1) $2/3NH_3 + O^{2-} \rightarrow 1/3N_2 + H_2O + 2e^-$ and (2) $1/2O_2 + 2e^- \rightarrow O^{2-}$ can be described as following equations:

$$i_{NH_3} = i^0_{NH_3} \exp\left[\frac{2\alpha_1 F\left(V - V^0_{NH_3}\right)}{RT}\right]$$

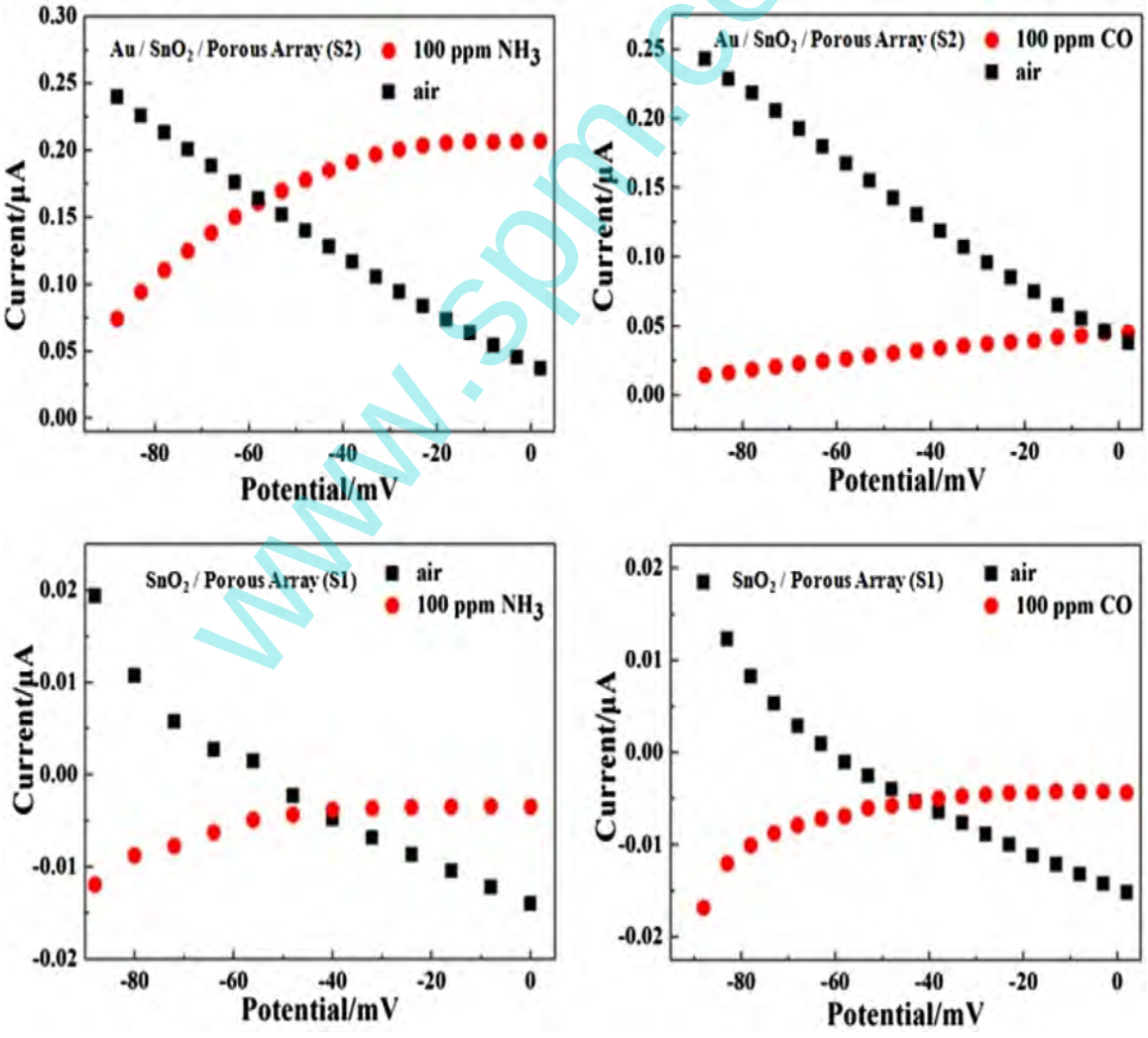

Fig. 13. Modified polarization curves (a) in 100 ppm CO and in air (b) in 100 ppm NH_3 and in air for sensor S1 and S2 operated at 650 °C.

$$i_{O_2} = i^0_{O_2} \exp\left[\frac{-2\alpha_2 F\left(V - V^0_{O_2}\right)}{RT}\right]$$

Where α and F represent the transfer coefficient and Faraday constant, i_0 and V_0 represent the exchange current density and electrode potential at equilibrium. R is the gas constant and T represents the temperature. The equalizations above could also be expressed as follow:

$$i^0_{NH_3} = B_1 C^m_{NH_3}$$

$$i^0_{O_2} = -B_2 C^n_{O_2}$$

Where B_1, B_2, n, and m are constants, C_{NH_3} and C_{O_2} are the concentration of NH_3 and O_2. When the electrochemical reactions reach the dynamic balance ($i_{NH_3} + i_{O_2} = 0$), the mixed potential was generated and could be represented by V_M:

$$V_M = V_O + mA\ln C_{O_2} - nA\ln C_{NH_3}$$

Here

$$V_0 = \frac{RT}{2(\alpha_1 + \alpha_2)F} \ln \frac{B_2}{B_1} + \frac{\alpha_1 V^0_{NH_3} + \alpha_2 V^0_{O_2}}{\alpha_1 + \alpha_2}$$

$$A = \frac{RT}{2(\alpha_1 + \alpha_2)F}$$

When C_{NH_3} is a constant, V_M could also be simplified as the following equations:

$$V_M = V_C + mA\ln C_{O_2} \quad (1)$$

It could be seen that V_M varies linearly to ln C_{O_2} from Eq. (1). In order to further determine whether the NH_3 sensor S2 comply with the mixed-potential theory, the measurements of sensor S2 to 100 ppm NH_3 at different concentrations of O_2 were carried out. Absolute value of the response to 100 ppm NH_3 decreases with increasing in O_2 concentration as indicated in Fig. 14(a). And the ΔV almost vary linear to the logarithm of O_2 concentrations with a positive slope in the examined range as shown in Fig. 14(b). The result further demonstrated that the sensor is accord with the mixed-potential mechanism.

From the perspective of practical applications, the repeatability and long term stability are also crucial evaluation parameters for a valuable sensor. The continuous response and recovery transients of sensor S2 switching on and off 100 ppm NH_3 at 650 °C has been tested and the corresponding result is shown in Fig. 15(a). It is clearly seen that the response of sensor S2 to 100 ppm NH_3 showed good repeatability in the examined eight-time circle. The long term stability of sensor S2 to 100 ppm NH_3 was measured at 650 °C as illustrated in Fig. 15(b). The change of the response to 100 ppm NH_3 was slightly, and the base line also showed good stability with ±2 mV change during a month measurement period.

4. Conclusion

In this work, the well-ordered porous array mounted with gold nanoparticles was successfully fabricated on the YSZ substrate using a solution-dipping PSs template strategy and vacuum evaporation technology. The optimal gold nanoparticle array was obtained when the thickness of gold layer was about 50 nm. The mixed-potential type NH_3 sensor based on processed YSZ inlaid with gold nanoparticles and SnO_2-SE was fabricated and the sensing characteristics were evaluated at elevated temperature. The response of the sensor S2 to 100 ppm NH_3 was approximately −63 mV at 650 °C, nearly thrice as much as S0. Meanwhile, the

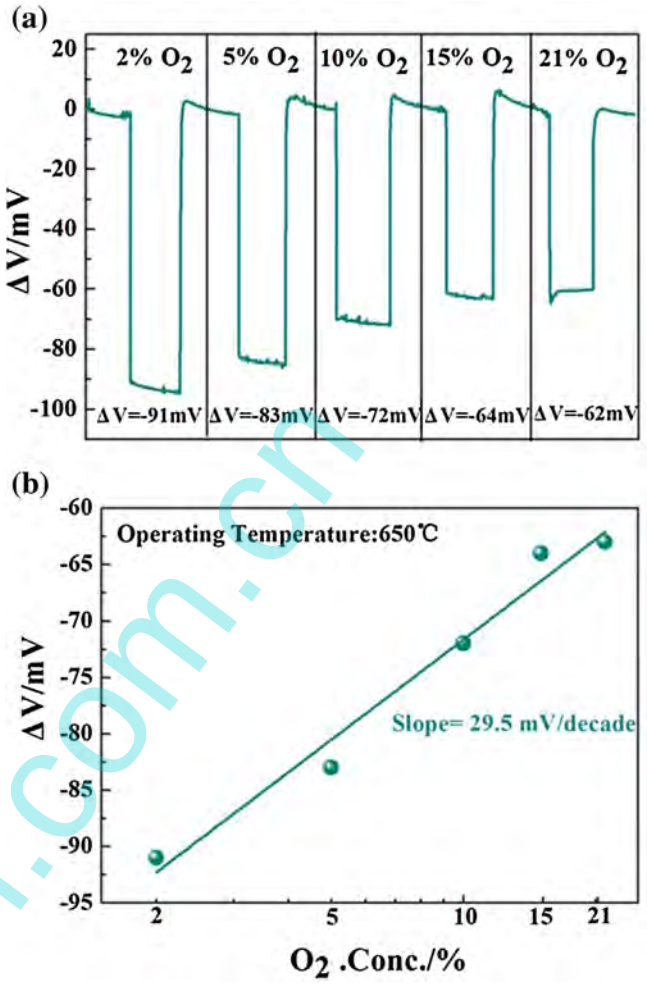

Fig. 14. (a) Responses of sensor S2 to 100 ppm NH_3 at different concentrations of O_2 at 650 °C; (b) dependence of the ΔV on the logarithm of O_2 concentrations.

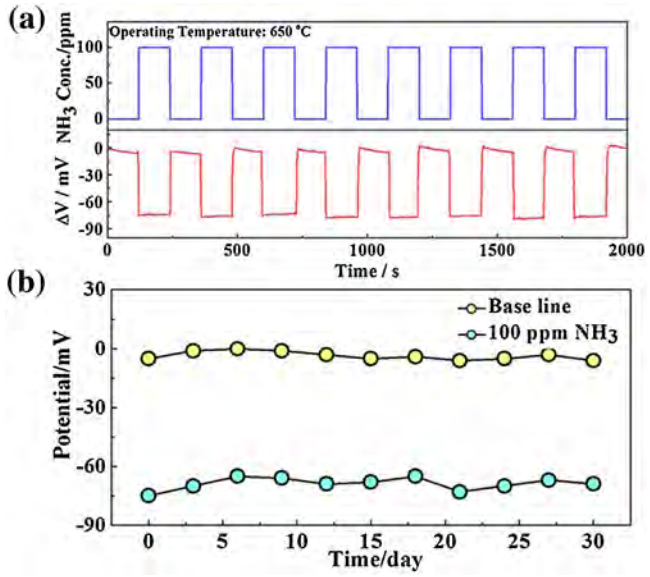

Fig. 15. (a) Continuous response–recovery transients of the sensor S2 switching on and off to 100 ppm NH_3 at 650 °C; (b) long-term stability at 650 °C for the sensor S2.

sensor S2 achieved a high sensitivity of −59.6 mV/decade to NH_3 in the range of 10–400 ppm at 650 °C. In addition, the sensor S2 also showed fast response and recovery times, improved selectivity, good repeatability and long term stability to NH_3 at 650 °C. All the improvements of the sensing properties were due to the high-performance TPB and gold nanoparticle on the YSZ substrate.

Acknowledgements

This work is supported by the National Nature Science Foundationof China (Nos. 61134010, 61327804, 61520106003, 61374218, 61533021, 61473132) Program for Chang Jiang Scholars and Innovative Research Team in University (No. IRT13018) and National High-Tech Research and Development Program of China (863 Program No. 2014AA06A505). Application and Basic Research of Jilin Province (2013010 2010JC). Project 2016028 Supported by Graduate Innovation Fund of Jilin University.

References

[1] B. Lee, J. Jung, C. Park, J. Lee, C. Hwang, Mixed potential NH_3 sensor with $LaCoO_3$ reference electrode, Sens. Actuators B: Chem. 176 (2013) 966–970.
[2] C.N. Xu, N. Miura, Y. Ishida, K. Matsuda, N. Yamazoe, Selective detection of NH_3 over NO in combustion exhausts by using Au and MoO_3 doubly promoted WO_3 element, Sens. Actuators B: Chem. 65 (2000) 163–165.
[3] P. Sekhar, E. Brosha, R. Mukundan, W. Li, M. Nelson, P. Palanisamy, F. Garzon, Application of commercial automotive sensor manufacturing methods for NO_x/NH_3 mixed potential sensors for on-board emissions control, Sens. Actuators B: Chem. 144 (2010) 112–119.
[4] N. Miura, G. Lu, N. Yamazoe, High-temperature potentiometric: amperometric NO_x sensors combining stabilized zirconia with mixed-metal oxide electrode, Sens. Actuators B: Chem. 52 (1998) 169–178.
[5] G. Lu, N. Miura, N. Yamazoe, High-temperature sensors for NO and NO_2 based on stabilized zirconia and spinel-type oxide electrodes, J. Mater. Chem. 7 (1997) 1445–1449.
[6] N. Miura, G. Lu, M. Ono, N. Yamazoe, Selective detection of NO by using an amperometric sensor basedon stabilized zirconia and oxide electrode, Solid State Ionics 117 (1999) 283–290.
[7] G. Lu, N. Miura, N. Yamazoe, Stabilized zirconia-based sensors using WO electrode for detection of NO or NO_2, Sens. Actuators B: Chem. 65 (2000) 125–127.
[8] F. Liu, Y. Guan, H. Sun, X. Xu, R. Sun, X. Liang, P. Sun, Y. Gao, G. Lu, YSZ-based NO_2 sensor utilizing hierarchical In_2O_3 electrode, Sens. Actuators B: Chem. 222 (2016) 698–706.
[9] P. Elumalai, V. Plashnitsa, Y. Fujio, N. Miura, Highly sensitive and selective stabilized zirconia-based mixed-potential-type propene sensor using NiO/Gold composite sensing-electrode, Sens. Actuators B: Chem. 144 (2010) 215–219.
[10] N. Wu, Q.Z. Chen, J. Xu, M. Chyu, S. Mao, Impedance-metric Pt/YSZ/Gold–Ga_2O_3 sensor for CO detection at high temperature, Sens. Actuators B: Chem. 110 (2005) 49–53.
[11] R. Sun, Y. Guan, X. Cheng, Y. Guan, X. Liang, J. Ma, P. Sun, Y. Sun, G. Lu, High performance three-phase boundary obtained by sand blasting technology for mixed-potential-type zirconia-based NO_2 sensors, Sens. Actuators B: Chem. 210 (2015) 91–95.
[12] X. Liang, S. Yang, J. Li, H. Zhang, Q. Diao, W. Zhao, G. Lu, Mixed-potential-type zirconia-based NO_2 sensor with high-performance three-phase boundary, Sens. Actuators B: Chem. 158 (2011) 1–8.
[13] Y. Guan, C. Li, X. Cheng, B. Wang, R. Sun, X. Liang, J. Zhao, H. Chen, G. Lu, Highly sensitive mixed-potential-type NO_2 sensor with YSZ processed using femtosecond laser direct writing technology, Sens. Actuators B: Chem. 198 (2014) 110–113.
[14] G. Duan, W. Cai, Y. Luo, F. Lv, J. Yang, Y. Li, Design and electrochemical fabrication of gold binary ordered micro/nanostructured porous arrays via step-by-step colloidal lithography, Langmuir 25 (2009) 2558–2562.
[15] F. Sun, W. Cai, Y. Li, B. Cao, Y. Lei, L. Zhang, Morphology-controlled growth of large-area two-dimensional ordered pore arrays, Adv. Funct. Mater. 14 (2014) 283–288.
[16] M. Ghanem, P. Bartlett, P. Groot, A. Zhukov, A double templated electro deposition method for the fabrication of arrays of metal nanodots, Electrochem. Commun. 6 (2004) 447–453.
[17] Y. Li, W. Cai, B. Cao, G. Duan, C. Li, F. Sun, H. Zeng, Morphology-controlled 2D ordered arrays by heating-induced deformation of 2D colloidal monolayer, J. Mater. Chem. 16 (2016) 609–612.
[18] A. Kosiorek, W. Kandulski, H. Glaczynska, M. Giersig, Fabrication of nanoscale rings, dots, and rods by combining shadow nanosphere lithography and annealed polystyrene nanosphere masks, Small 1 (2005) 439–444.
[19] B. Wang, F. Liu, X. Yang, Y. Guan, C. Ma, X. Hao, X. Liang, F. Liu, P. Sun, T. Zhang, G. Lu, Fabrication of well-ordered three-phase boundary with nanostructure pore array for mixed potential-type zirconia-based NO_2 sensor, ACS Appl. Mater. Interfaces 8 (2016) 16752–16760.
[20] D. Luna-Moreno, D. Monzon-Hernandez, S. Calixto-Carrera, R. Espinosa-Luna, Tailored Pd–Gold layer produced by conventional evaporation process for hydrogen sensing, Opt. Laser. Eng. 49 (2011) 693–697.
[21] C. Brinker, Y. Lu, A. Sellinger, H. Fan, Evaporation-induced self-assembly: nanostructures made easy, Adv. Mater. 11 (1999) 579–585.
[22] X. Cheng, C. Wang, B. Wang, R. Sun, Y. Guan, Y. Sun, X. Liang, P. Sun, G. Lu, Mixed-potential-type YSZ-based sensor with nano-structured NiO and porous TPB processed with pore-formers using coating technique, Sens. Actuators B: Chem. 221 (2015) 1321–1329.
[23] P. Montmeat, J.C. Marchand, R. Lalauze, J.P. Viricelle, G. Tournier, C. Pijolat, Physico-chemical contribution of gold metallic particles to the action of oxygen on tin dioxide sensors, Sens. Actuators B: Chem. 95 (2003) 83–89.
[24] J. Zhang, X.H. Liu, S.H. Wu, M.J. Xu, X.Z. Guo, S.R. Wang, Au nanoparticle-decorated porous SnO_2 hollow spheres: a new model for a chemical sensor, J. Mater. Chem. 20 (2010) 6453–6459.
[25] S.D. Bakrania, M.S. Wooldridge, The effects of the location of Au additives on combustion-generated SnO_2 nanopowders for CO gas sensing, Sensors 10 (2010) 7002–7017.
[26] H.W. Wang, C.L. Wang, H. Yan, H. Yi, J.L. Lu, Precisely-controlled synthesis of Au@Pd core–shell bimetallic catalyst via atomic layer deposition for selective oxidation of benzyl alcohol, J. Catal. 324 (2015) 59–68.
[27] Y. Zhang, Q. Xiang, J. Xu, P.C. Xu, Q.Y. Pan, F. Li, Self-assemblies of Pd nanoparticles on the surfaces of single crystal ZnO nanowires for chemical sensors with enhanced performances, J. Mater. Chem. 19 (2009) 4701–4706.
[28] K.P. Kamloth, Semiconductor junction gas sensors, Chem. Rev. 108 (2008) 367–399.
[29] B. Swierkosz, Nano-Au/oxide support catalysts in oxidation reactions: provenance of active oxygen species, Catal. Today 112 (2006) 3–7.
[30] M. Schubert, S. Hackenberg, A. van Veen, M. Muhler, V. Plzak, R. Behm, CO oxidation over supported gold catalysts—inert and active support materials and their role for the oxygen supply during reaction, J. Catal. 197 (2001) 113–122.
[31] Q. Yao, C.L. Wang, H.W. Wang, H. Yan, J.L. Lu, Revisiting the Au particle size effect on TiO_2-coated Au/TiO_2 catalysts in CO oxidation reaction, J. Phys. Chem. C 120 (2016) 9174–9183.
[32] V. Plashnitsa, P. Elumalai, Y. Fujio, T. Kawaguchi, N. Miura, Spontaneous gradual accumulation of hexagonally-aligned nano-silica on gold nanoparticles embedded in stabilized zirconia: a pathway from catalytic to NH_3 sensing performance, Nanoscale 3 (2011) 2286–2293.
[33] N. Miura, T. Sato, S. Anggraini, H. Ikeda, S. Zhuiykov, A review of mixed-potential type zirconia-based gas sensors, Ionics 20 (2014) 901–925.
[34] F. Liu, R. Sun, Y. Guan, X. Cheng, H. Zhang, Y. Guan, X. Liang, P. Sun, G. Lu, Mixed-potential type NH_3 sensor based on stabilized zirconia and $Ni_3V_2O_8$ sensing electrode, Sens. Actuators B: Chem. 210 (2015) 795–802.
[35] F. Liu, Y. Guan, M. Dai, H. Zhang, Y. Guan, R. Sun, X. Liang, P. Sun, F. Liu, G. Lu, High performance mixed-potential type NO_2 sensors based on three-dimensional TPB and $Co_3V_2O_8$ sensing electrode, Sens. Actuators B: Chem. 216 (2015) 121–127.
[36] D.S. Kamin, M. Fleischer, R. Moos, Half-cell potential analysis of an ammonia sensor with the electrochemical cell Au | YSZ | Au, V_2O_5-WO_3-TiO_2, Sensors 13 (2013) 4760–4780.
[37] T. Sato, H. Iked, N. Miura, Mixed-potential type zirconia-based NH_3 sensor using SnO_2-disk sensing-electrode attached with sputtered gold, ECS Electrochem. Lett. 3 (2014) B13–B15.

Biographies

Bin Wang received the B.Eng. degree in department of electronic science and technology in 2015. He is currently studying for his M.E. Sci. degree in College of Electronic Science and Engineering, Jilin University, China.

Shiting Yao received the B.Eng. degree in department of Changchun University of Science and Technology in 2014. She is currently studying for her electronic Sci. degree in College of Electronic Science and Engineering, Jilin University, China.

Fangmeng Liu received his B.S. degree in 2009 from College of Chemistry, Liaocheng University and M.S. degree in 2012 from Northeast Forestry University in China. Currently he is studying for his Ph.D. degree in College of Electronic Science and Engineering, Jilin University, China.

Yehui Guan received the B.Eng.degree in department of electronic science and technology in 2014. He is currently studying for his M.E. Sci. degree in College of Electronic Science and Engineering, Jilin University, China.

Xidong Hao, received the B.Eng. degree in department of electronic science and technology in 2016. He is currently studying for his M.E. Sci. degree in College of Electronic Science and Engineering, Jilin University, China.

Xishuang Liang received the B. Eng. degree in Department of Electronic Science and Technology in 2004. He received his Doctor's degree in College of Electronic Science and Engineering at Jilin University in 2009. Now he is an associate professor of Jilin University, China. His current research is solid electrolyte gas sensor.

Fengmin Liu received the BE degree in Department of Electronic Science and Technology in 2000. She received his Doctor's degree in College of Electronic Science and Engineering at Jilin University in 2005. Now she is a professor in Jilin University, China. Her current research is preparation and application of semiconductor oxide, especial in gas sensor and solar cell.

Peng Sun received his PhD degree from the Electronics Science and Engineering department, Jilin University, China in 2014. Now, he is engaged in the synthesis and characterization of the semiconducting functional materials and gas sensors.

Yue Wang received his PhD degree from Jilin University, China in 1991. He then joined the State Key Lab of Supramolecular Structure and Materials in Jilin University as an assistant professor. He is currently a full professor in the State Key Lab of Supramolecular Structure and Materials in Jilin University. His research interests are organic electroluminescence, thin film transistor and solar cell materials and devices.

Hongwei Song received his Ph.D. degree from Changchun Ins. of Physics, CAS in 1996. From 1996 to 2000, he worked as a postdoctor in Ins. of Physics, CAS, Nagoya Ins. of Technology and Univ. of California at Berkeley, respectively. In 2001, he gained One hundred Talent Youth Project and became a professor of CIOMP. In 2008, he won National Talent Youth Project of China. He is currently working as a professor in Jilin University. So far, he has published more than 160 SCI journal papers and two book chapters. His research interests concern on the synthesis of nanomaterials, their optical and electrical properties and biological applications.

Geyu Lu received the B.Sci. degree in electronic sciences in 1985 and the M.S. degree in 1988 from Jilin University in China and the Dr. Eng. degree in 1998 from Kyushu University in Japan. Now he is a professor of Jilin University, China. His current research interests include the development of chemical sensors and the application of the function materials.